Research Article

Impacts of temperature-dependent viscosity and variable Prandtl number on forced convective Falkner–Skan flow of Williamson nanofluid

H. Thameem Basha[1] · R. Sivaraj[1] · A. Subramanyam Reddy[1] · Ali J. Chamkha[2] · M. Tilioua[3]

Abstract
Fluid viscosity is considered as constant in several boundary layer analyses, but this fluid property can change remarkably when the temperature difference exists in the boundary layer. The Prandtl number and Schmidt number can also change significantly as the fluid viscosity changes depending on temperature. Therefore, this framework is exploring the consequences of varying viscosity and varying Prandtl number on Falkner–Skan flow of Williamson nanofluid over a wedge, plate and stagnation point. The Buongiorno nanofluid model has been employed to manifest the fluid transport properties of the Williamson nanofluid. Similarity transformations are utilized to transform the governing equations into ordinary differential equation and solved numerically using Runge–Kutta (RK) Fehlberg method. Williamson fluid velocity, temperature, concentration, skin friction factor, rate of heat transfer and rate of mass transfer are investigated with emerging parameters, and the outcomes are presented graphically. Computed results manifest that the Williamson nanofluid expresses the opposite nature in velocity and temperature for higher values of Weissenberg number parameter. Positive values of variable viscosity parameter diminish the significance of variable Prandtl number and variable Schmidt number in the boundary layer. Furthermore, it is noticed that the Williamson nanofluid temperature is higher over a plate compared with wedge and stagnation point cases.

Keywords Williamson nanofluid · Falkner–Skan flow · Variable viscosity · Variable Prandtl number · Wedge/plate/stagnation point

Nomenclature

x, y	Cartesian coordinate system [m]
u, v	Velocity components $[\mathrm{m\,s^{-1}}]$
T	Temperature of fluid [K]
T_w	Temperature at the surface [K]
T_∞	Ambient temperature [K]
C	Nanoparticles concentration
C_w	Concentration at the surface
C_∞	Ambient nanoparticles concentration
D_B	Brownian diffusion coefficient $[\mathrm{m^2/s}]$
D_T	Thermophoresis diffusion coefficient $[\mathrm{m^2/s}]$
N_B	Brownian motion parameter
N_T	Thermophoresis parameter
b	Constant
C_f^*	Skin friction coefficient
Nu^*	Nusselt number
Sh^*	Sherwood number
Pr_∞	Prandtl number
Re	Local Reynolds number
k	Thermal conductivity [W/m K]
m	Hartree pressure gradient parameter
f	Dimensionless stream function
We	Weissenberg number
Sc_∞	Schmidt number

✉ R. Sivaraj, sivaraj.kpm@gmail.com | [1]Department of Mathematics, School of Advanced Sciences, Vellore Institute of Technology, Vellore 632014, India. [2]Mechanical Engineering Department, Prince Sultan Endowment for Energy and Environment, Prince Mohammad Bin Fahd University, Al-Khobar 31952, Saudi Arabia. [3]M2I Laboratory, MAMCS Group, FST Errachidia, Moulay Ismal University of Mekns, P.O. Box: 509, Boutalamine 52000, Errachidia, Morocco.

E_c Eckert number
$(\rho C)_p$ Heat capacity of nanofluid
$(\rho C)_f$ Heat capacity of base fluid
C_p Specific heat at constant pressure $\left[\text{J kg}^{-1}\,\text{K}^{-1}\right]$
Ks Slip parameter
Kn_x Local Knudsen number
u_{Slip} Velocity slip
$\frac{\partial u}{\partial n}$ Velocity gradient normal to the surface
$\frac{\partial T}{\partial S}$ Temperature gradient to the wall

Greek symbols

Γ Relaxation time [s]
μ Viscosity [N s/m^2]
μ_∞ Infinite viscosity [N s/m^2]
ν Kinematic viscosity $\left[\text{m}^2/\text{s}\right]$
ψ Stream function
θ Dimensionless temperature
χ Dimensionless concentration
η Dimensionless variable
α^* Thermal diffusivity [m^{2}s^{-1}]
τ Ratio between particle and base fluid
β_1 Total wedge angle
ρ_∞ Fluid density $\left[\text{kg /m}^3\right]$
λ Parameter
ϖ Thermal property
θ_r Variable viscosity parameter
σ_M Accommodation coefficient of tangential momentum
σ_T Accommodation coefficient of thermal
λ_0 Molecular mean free path
γ Ratio of specific heat

1 Introduction

Rapid heat dissipation is significant in enhancing the efficiency of industrial processes, power generation, electronics, and automobile radiators due to a growing demand for energy conservation. Engineers and researchers have made many attempts to increase the performance of heat dissipation. Due to less capability of normal heat transfer, the fluids such as ethylene glycol, oil, and water are not enough to meet today's needs. Nanofluids are the new generation working fluids with high potential which are used in the industries. Nanofluid is a colloidal mixture of nanosized particles (less than 100 nm) in regular heat transfer fluid which exhibit better heat dissipation than ordinary fluids. Such a new class of high heat transfer fluids was first proposed by Choi et al. [1]. Numerous investigations have been carried out to explore the transport characteristics and thermal properties of the nanofluids that most of them have divulged a positive effect of nanofluids on the heat dissipation. Nanofluid was initially used

only for heat transfer applications, but in recent days it is widely employed in biomedical engineering (drug delivery, vivo therapy, photodynamic therapy, neuro-electronic interfaces, and chromatography), renewable energy (solar thermoelectric devices, solar collector, biomass and geothermal), etc. Several models have been introduced to study the nanofluid; the Buongiorno model is one of the nanofluid models which are adopted by many researchers to analyze the nanofluid. Buongiorno [2] model consists of the momentum, heat and mass transport equations with the influence of Brownian motion and thermophoretic diffusivity. It is noteworthy that the Brownian motion has a higher impact when Joule heating is significant and the effect of thermophoresis should be ignored when considering the energy flux generated by the mass flux caused by the temperature gradient. Recently, Animasaun et al. [3] delivered a detailed theoretical review of Brownian motion in various nanofluids and pointed out that the collision between the particles is caused by the increase in the Brownian motion of the particles. Wakif et al. [4] provided a technical note to emphasize the essential role of partial migration and the significance of thermophoresis in various fluids and noted that the impact of thermophoresis on non-Newtonian fluids is higher than that of Newtonian fluids. Khan et al. [5] utilized the Buongiorno nanofluid model to explore fluid transport properties and entropy generation of tangent hyperbolic nanofluid with nonlinear convection and observed that varying thermophoretic parameter enhances temperature and mass transfer of nanofluid. Ghadikolaei et al. [6] scrutinized the impact of nonlinear radiation on magneto Eyring–Powell nanofluid by using Buongiorno nanofluid model and found that increasing values of Brownian motion parameter declines the mass transfer. Ahmed et al. [7] numerically investigated the Maxwell nanofluid over a permeable disk in the presence of Brownian motion and thermophoresis. Few studies on Buongiorno nanofluid model are cited in Refs.[8–12]

When the shear stress and shear rate of the fluid are nonlinear, the fluid becomes non-Newtonian and this fluid is classified into visco-elastic fluid, dilatant, pseudoplastic, micropolar fluid, and Bingham plastic. The boundary layer flow with pseudoplastic fluids has a significant application in bio-science and engineering systems due to its wide uses in biological materials (blood, saliva), chemical materials (polymer fluids, pharmaceutical chemicals), food processing (ketchup, yogurt), flow in journal bearings, solar collectors, etc. The Navier–Stokes equations are unable to elucidate the flow characteristics of non-Newtonian fluids because of the complex rheological properties of non-Newtonian fluids. To overcome this shortcoming, many researchers have proposed several rheological models such as Cross fluid, Carreau fluid, Maxwell fluid, Walter's B fluid, Casson fluid and Williamson fluid. Several authors investigated different

types of non-Newtonian models in various aspects [13–17]. Williamson fluid is one of the non-Newtonian fluids, and this model was proposed by Williamson [18]. It is noticed that this fluid model is a classic example of visco-elastic shear thinning fluid. It is also noticed that Williamson fluid model has represented the exact characteristic of pseudoplastic fluids. Furthermore, the viscosity of the Williamson fluids decreases while the shear stress rate is improved. Abegunrin et al. [19] investigated the influence of the quartic autocatalytic on chemically reacting Williamson nanofluid over an upper surface of a horizontal paraboloid of revolution and noticed that Weissenberg number has less impact on the fluid transport properties. Hashim et al. [20] scrutinized the time-dependent Williamson nanofluid over a disk with the impact of varying fluid temperature and found that high-thermal-conductivity parameter uplifts Williamson fluid temperature. Abegunrin and Animasaun [21] addressed the fluid transport properties of Williamson fluid in the presence and absence of partial slip and thermal jump cases and observed that the horizontal velocity increases in the presence of partial slip and thermal jump. Khan et al. [22] examined the variable viscosity and Lorentz force impacts on Williamson nanofluid in the presence of dual stratification effect.

In heat and mass transfer characteristics, convection is a mechanism which is classified into free, mixed and forced. Forced convection occurs when the convection is driven by an external force like a fan, pump and suction devices. This mechanism has great potential in many practical engineering applications like growth in electroactive biofilms [23], wire-coil inserts [24], vapor explosions [25], solar energy [26], electronic device cooling, cooling of gas turbine blades and rocket propulsion. Lin and Lin [27] examined forced convective Falkner–Skan flow over a wedge, plate, and stagnation of a flat plate and introduced a parameter to investigate the fluid of any Prandtl number. Bianco [28] investigated the forced convection in a circular tube with water-based Al_2O_3 nanofluid and observed that uplifting the nanoparticle concentration tends to enhance the heat transfer. Sheikholeslami [29] employed lattice Boltzmann method to explore the characteristics of heat transfer and Lorentz force in a porous cavity with forced convection. Rahman et al. [30] numerically studied the forced convective flow by accounting the influence of varying viscosity and varying Prandtl number and pointed out that static wedge has a higher temperature than the moving wedge. Chamkha et al. [31] investigated the influence of linear radiation on Newtonian fluid over a non-isothermal moving wedge and found that by varying the Hartree pressure gradient parameter ($\beta = 0.0, 0.5, 1.0$) declines the Newtonian fluid temperature. Uddin et al. [32] scrutinized the impact of variable fluid properties on the forced convective flow of nanofluid by using Buongiorno nanofluid

model and noticed that Falkner–Skan flow parameter has a high temperature and concentration at $m = 0$(flat plate) compared with Falkner–Skan flow parameter $m = 1$(stagnation point). Further studies on forced convective flow can be found in Refs. [33–35]. The solutions for nonlinear Boundary Value Problems (BVPs) play a significant role in characterizing many science and engineering problems. It can be seen that most of the nonlinear BVPs are Partial Differential Equations (PDEs). An important issue on solving the nonlinear PDEs is computational complexity since most of the boundary layer equations are highly nonlinear and coupled. When the PDEs are converted to the Ordinary Differential Equations (ODEs) using the similarity variable, computational complexity is reduced, and the solution obtained by the PDEs becomes similar to the ODEs solution. As a result, many researchers have used similarity variables to solve highly nonlinear BVPs.

The present work reports the forced convective Falkner–Skan flow of Williamson nanofluid in the presence of thermal jump and viscous dissipation. The variable viscosity, variable Prandtl number, and variable Schmidt number are considered to investigate the fluid characteristic of Williamson nanofluid. The fluid transport equations are modeled by using Buongiorno nanofluid model. It is to be noted that the employed similarity transformation is suitable for any fluid Prandtl number. RK Fehlberg method is adopted as a computational tool for characterizing the non-dimensional governing equations. Influence of diverse pertinent parameters on the velocity, temperature and concentration is analyzed through the graphs. To the best of the authors' knowledge, no study has been performed to explore the effects of variable viscosity, variable Prandtl number, and variable Schmidt number on Williamson nanofluid over three different geometry cases. Owing to the significance of this kind of problems, the present study intends to manifest answers to the following research questions: (i) What are the characteristics of wall Prandtl number and the wall Schmidt number over three different geometries due to the impact of variable viscosity and thermophoresis? (ii) On which geometry, the Williamson nanofluid has a higher heat transfer rate? (iii) What is the impact of velocity slip and thermal jump on Williamson nanofluid flow over wedge, plate, and stagnation point?

2 Mathematical formulation

We consider two-dimensional (x, y) forced convective Falkner–Skan flow of Williamson nanofluid over a wedge, plate and stagnation point of flat plate, as demonstrated in Fig. 1. It is assumed that the velocity of the potential flow away from the boundary layer is $u_\infty = bx^m$ where b is

Fig. 1 Flow geometry for wedge, plate and stagnation point
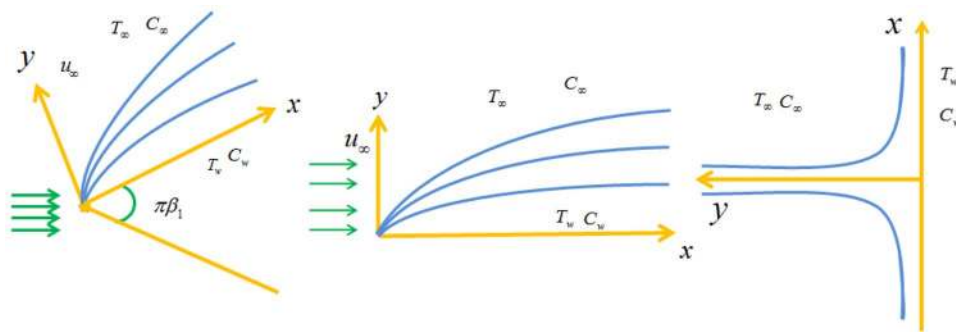
the constant. Here, $m = \frac{\beta_1}{2-\beta_1}$ is the Hartree pressure gradient. $\beta_1 = 0$, 0.5 and 1 represents the flow over a plate, wedge and stagnation point of a flat plate, respectively. The temperature (T_w) and concentration (C_w) of the wall are fixed, and it is higher than the ambient temperature (T_∞) and ambient concentration (C_∞).

Based on the above settings, the flow assumptions are

- Laminar, steady, incompressible, forced convective flow of Williamson nanofluid is considered.
- The body force is neglected in the momentum equation.
- Thermal jump is considered at the boundary.
- The dissipation of Williamson nanofluid is considered in the energy equation.
- Buongiorno nanofluid model is employed to model the governing equation.

Within the framework of the aforementioned suppositions, the governing equations are [8, 18, 26, 27]

$$\frac{\partial u}{\partial x} + \frac{\partial v}{\partial y} = 0, \tag{1}$$

$$u\frac{\partial u}{\partial x} + v\frac{\partial u}{\partial y} = u_\infty \frac{du_\infty}{dx} + \frac{1}{\rho_\infty}\left(\mu(T)\frac{\partial u}{\partial y}\right) \\ + \frac{\Gamma\sqrt{2}}{\rho_\infty}\left(\frac{\partial}{\partial y}\left(\mu(T)\frac{\partial u}{\partial y}\right)\frac{\partial u}{\partial y}\right), \tag{2}$$

$$u\frac{\partial T}{\partial x} + v\frac{\partial T}{\partial y} = \alpha^*\frac{\partial^2 T}{\partial y^2} + \tau\left[D_B\frac{\partial T}{\partial y}\frac{\partial C}{\partial y} + \frac{D_T}{T_\infty}\left(\frac{\partial T}{\partial y}\right)^2\right] \\ + \frac{\mu(T)}{(\rho_\infty C_P)_f}\left(\frac{\partial u}{\partial y}\right)^2 + \frac{\mu(T)}{(\rho_\infty C_P)_f}\Gamma\left(\frac{\partial u}{\partial y}\right)^3, \tag{3}$$

$$u\frac{\partial C}{\partial x} + v\frac{\partial C}{\partial y} = D_B\frac{\partial^2 C}{\partial y^2} + \frac{D_T}{T_\infty}\frac{\partial^2 T}{\partial y^2}. \tag{4}$$

The boundary conditions are [8, 26, 30]

$$u = u_{\text{Slip}} = \lambda_0\left(\frac{\partial u}{\partial n} + \frac{\Gamma}{\sqrt{2}}\left(\frac{\partial u}{\partial n}\right)^2\right)\left(\frac{2-\sigma_M}{\sigma_M}\right) + \frac{3v}{4T_g}\frac{\partial T}{\partial S},$$

$$v = 0, \; T_{\text{Jump}} = T_g - T_w = \lambda_0\frac{2\gamma}{\gamma+1}\frac{\partial T}{\partial n}\left(\frac{2-\sigma_T}{\sigma_T}\right)\frac{1}{\text{Pr}_\infty},$$

$$D_B\frac{\partial C}{\partial y} + \frac{D_T}{T_\infty}\frac{\partial T}{\partial y} = 0 \quad \text{at } y = 0,$$

$$u = u_\infty, \; T \to T_\infty, C \to C_\infty \qquad \text{as } y \to \infty. \tag{5}$$

where $v = \frac{\mu}{\rho}$, $\alpha^* = \frac{k}{(\rho C_p)_f}$, $\tau = \frac{(\rho C_p)_p}{(\rho C_p)_f}$.

Temperature variation notably affects the nanofluid velocity and the rate of heat transfer. As a consequence, to accurately infer the nanofluid flow and rate of heat transfer, the nanofluid viscosity is considered as inversely proportional to nanofluid temperature.

Therefore, this can be expressed as [8, 30],

$$\frac{1}{\mu} = \frac{\left(1 + \varpi\left(T - T_\infty\right)\right)}{\mu_\infty}, \tag{6}$$

Eq. (6) can be rewritten as,

$$\frac{1}{\mu} = B\left(T - T_r\right), \tag{7}$$

where μ_∞ and ϖ are dynamic viscosity and thermal property of the nanofluid, respectively. $B = \frac{\varpi}{\mu_\infty}$ and $T_r = \frac{\varpi T_\infty - 1}{\varpi}$. It is essential to note that the positive values of B correspond to liquid and the negative values of B correspond to gases.

Hence, the dimensionless temperature can be expressed as

$$\theta = \frac{T - T_r}{T_w - T_\infty} + \theta_r, \tag{8}$$

where $\theta_r = \frac{T_r - T_\infty}{T_w - T_\infty} = -\frac{1}{\varpi(T_w - T_\infty)}$ is the variable viscosity parameter. It is mentioned that the $\theta_r > 0$ represents liquid and $\theta_r < 0$ represents gases.

Using Eqs. (7) and (8), the dynamic viscosity becomes

$$\mu = \left(\frac{\theta_r}{\theta_r - \theta}\right)\mu_\infty. \tag{9}$$

A parameter λ is given by Lin and Lin [27] which is used to apply for any fluid Prandtl number $\lambda = \delta\sqrt{Re}$, where $Re = \frac{u_\infty x}{v_\infty}$ is Reynolds number, $\delta = \frac{\sqrt{Pr_\infty}}{(1+Pr_\infty)^n}, n = \frac{1}{6}$ for plate, wedge and stagnation of flat plate, Pr_∞ is Prandtl number.

Now, the similarity transformations are introduced as follows:

$$\left.\begin{array}{l}
\eta = \left(\frac{y}{x}\right)\lambda, \\
f(\eta) = \frac{\psi(x,y)}{\alpha^* \lambda}, \\
u = \frac{f'(\eta)bx^m}{(1+Pr_\infty)^{2n}}, \\
v = -\left(\frac{\alpha^*}{x}\right)\lambda\left[\frac{m+1}{2}f(\eta) + \frac{m-1}{2}\eta f'(\eta)\right], \\
T = (T_w - T_\infty)\theta(\eta) + T_\infty, \\
C = (C_w - C_\infty)\chi(\eta) + C_\infty.
\end{array}\right\} \tag{10}$$

Based on Eq. (6), Eqs. (2)–(4) are transformed to

$$Pr_\infty f''' \left[1 + 2We f''\left(\frac{Pr_\infty}{(1+Pr_\infty)^{3n}}\right)\right]$$

$$+ \left[1 + We f''\left(\frac{Pr_\infty}{(1+Pr_\infty)^{3n}}\right)\right]$$

$$\frac{Pr_\infty \theta' f''}{(\theta_r - \theta)} + \left(\frac{m+1}{2}\right)f f''\left(1 - \frac{\theta}{\theta_r}\right)$$

$$+ m\left((1+Pr_\infty)^{4n} - (f')^2\right)\left(1 - \frac{\theta}{\theta_r}\right) = 0, \tag{11}$$

$$\theta'' + Pr_\infty N_B \theta' \chi' + Pr_\infty N_T (\theta')^2 + \left(\frac{m+1}{2}\right)f\theta'$$

$$+ \frac{Pr_\infty}{(1+Pr_\infty)^{4n}}E_C(f'')^2 \frac{1}{\left(1 - \frac{\theta}{\theta_r}\right)} \tag{12}$$

$$\left[1 + We f''\left(\frac{Pr_\infty}{\sqrt{2}(1+Pr_\infty)^{3n}}\right)\right] = 0,$$

$$\chi'' + \left(\frac{m+1}{2}\right)f\chi' \frac{Sc_\infty}{Pr_\infty} + \frac{N_T}{N_B}\theta'' = 0. \tag{13}$$

Velocity boundary can be written as [8],

$$f'(\eta) = \frac{\sqrt{Pr_\infty}f''(\eta)}{(1+Pr_\infty)^n}\left(\frac{2-\sigma_M}{\sigma_M}\right)Kn_x\sqrt{Re} = \frac{\sqrt{Pr_\infty}K_s f''(\eta)}{(1+Pr_\infty)^n}. \tag{14}$$

where $K_s = Kn_x\left(\frac{2-\sigma_M}{\sigma_M}\right)\sqrt{Re}$ is the slip parameter and $Kn_x = \frac{\lambda_0}{x}$ is the local Knudsen number.

Thermal boundary can be written as

$$\theta(\eta) = 1 + \frac{2\gamma}{\gamma+1}\frac{1}{\sqrt{Pr_\infty}}\frac{\theta'(\eta)}{(1+Pr_\infty)^n}\left(\frac{2-\sigma_M}{\sigma_M}\right)Kn_x\sqrt{Re},$$

$$\theta(\eta) = 1 + \frac{2\gamma}{\gamma+1}\frac{1}{\sqrt{Pr_\infty}}\frac{K_s\theta'(\eta)}{(1+Pr_\infty)^n}. \tag{15}$$

Here, it is assumed that momentum and thermal accommodation coefficients are equal, i.e., $\sigma_M = \sigma_T$.

Using Eqs. (14) and (15), then the transformed boundary condition becomes

$$f(\eta) = 0, f'(\eta) = \frac{\sqrt{Pr_\infty}K_s f''(\eta)}{(1+Pr_\infty)^n}\left(1 + \frac{We}{2}\frac{\sqrt{Pr_\infty}f''(\eta)}{(1+Pr_\infty)^{3n}}\right),$$

$$\theta(\eta) = 1 + \frac{2\gamma}{\gamma+1}\frac{1}{\sqrt{Pr_\infty}}\frac{K_s\theta'(\eta)}{(1+Pr_\infty)^n}, \quad N_B\chi'(\eta) + N_T\theta'(\eta) = 0 \text{ at } \eta = 0,$$

$$f'(\eta) = (1+Pr_\infty)^{2n}, \quad \theta(\eta) \to 0, \quad \chi(\eta) \to 0 \text{ as } \eta \to \infty. \tag{16}$$

where $We = \Gamma\sqrt{\frac{2u_\infty^3}{v_\infty x}}$, $N_T = \frac{\tau D_T(T_w - T_\infty)}{T_\infty v_\infty}$, $E_C = \frac{u_\infty^2}{(C_p)_f(T_w - T_\infty)}$, $N_B = \frac{\tau D_B(C_w - C_\infty)}{v_\infty}$, $Pr_\infty = \frac{\mu C_P}{k}$ and $Sc_\infty = \frac{v_\infty}{D_B}$.

It is noticed that the viscosity of the nanofluid within the boundary layer varies, based on that the Prandtl number and Schmidt number also changes. Due to this reason, the Prandtl number and Schmidt number are considered as variables.

Variable Prandtl number can be written as [8, 30],

$$Pr_v = \frac{\mu C_P}{k} = \frac{\left(\frac{\theta_r}{\theta_r - \theta}\right)\mu_\infty C_p}{k} = \frac{1}{\left(1 - \frac{\theta}{\theta_r}\right)}Pr_\infty. \tag{17}$$

Variable Schmidt number can be written as,

$$Sc_v = \frac{\mu}{\rho_\infty D_B} = \frac{\left(\frac{\theta_r}{\theta_r - \theta}\right)\mu_\infty}{\rho_\infty D_B} = \frac{\left(\frac{\theta_r}{\theta_r - \theta}\right)v_\infty}{D_B} = \frac{1}{\left(1 - \frac{\theta}{\theta_r}\right)}Sc_\infty. \tag{18}$$

It is mentioned that when $\theta_r (\theta_r \to \infty)$ has a higher value, the Pr_v and Pr_∞ are equal. A similar behavior is observed for Schmidt number.

Based on Eqs. (13) and (14), Eqs. (11)–(14) can be written as

Table 1 Comparison result of C_f^* with dsolve (Maple)

Parameter θ_r	$C_f^* \mathrm{Re}^{-1/2}$					
	Plate		Wedge		Stagnation point	
	RKF	Dsolve	RKF	Dsolve	RKF	Dsolve
	Method	(Maple)	Method	(Maple)	Method	(Maple)
2	0.905262	0.905262	1.448131	1.448132	1.297994	1.297995
3	0.761932	0.761932	1.184679	1.184683	1.354163	1.354164
4	0.705068	0.705068	1.079093	1.079093	1.445044	1.445046
5	0.674288	0.674289	1.022070	1.022070	1.616838	1.616839
6	0.654953	0.654957	0.986375	0.986375	1.297994	1.297994

Table 2 Comparison result of Nu^* with dsolve (Maple)

Parameter N_T	$Nu^* \mathrm{Re}^{-1/2}\delta^{-1}$					
	Plate		Wedge		Stagnation point	
	RKF	Dsolve	RKF	Dsolve	RKF	Dsolve
	Method	(Maple)	Method	(Maple)	Method	(Maple)
0.1	0.261681	0.261681	0.379869	0.379869	0.561115	0.561115
0.3	0.236547	0.236547	0.343955	0.343956	0.512008	0.512009
0.5	0.210186	0.210186	0.306561	0.306562	0.461037	0.461038
0.7	0.182640	0.182639	0.267930	0.267930	0.408644	0.408644
1.0	0.139513	0.139510	0.208814	0.208814	0.329213	0.329217

$$\mathrm{Pr}_v\left(1-\frac{\theta}{\theta_r}\right)f'''\left[1+2\,Wef''\left(\frac{\mathrm{Pr}_v\left(1-\frac{\theta}{\theta_r}\right)}{\left(1+\mathrm{Pr}_v\left(1-\frac{\theta}{\theta_r}\right)\right)^{3n}}\right)\right]$$

$$+\left[1+Wef''\left(\frac{\mathrm{Pr}_v\left(1-\frac{\theta}{\theta_r}\right)}{\left(1+\mathrm{Pr}_v\left(1-\frac{\theta}{\theta_r}\right)\right)^{3n}}\right)\right]$$

$$\frac{\mathrm{Pr}_v\left(1-\frac{\theta}{\theta_r}\right)\theta'f''}{(\theta_r-\theta)}+\left(\frac{m+1}{2}\right)f f''$$

$$\left(1-\frac{\theta}{\theta_r}\right)+m\left(\left(1+\mathrm{Pr}_v\left(1-\frac{\theta}{\theta_r}\right)\right)^{4n}-(f')^2\right)\left(1-\frac{\theta}{\theta_r}\right)=0,$$

$$(19)$$

$$\theta''+\mathrm{Pr}_v\left(1-\frac{\theta}{\theta_r}\right)N_B\theta'\chi'+\mathrm{Pr}_v\left(1-\frac{\theta}{\theta_r}\right)N_T(\theta')^2+\left(\frac{m+1}{2}\right)f\theta'$$

$$+\frac{\mathrm{Pr}_v\left(1-\frac{\theta}{\theta_r}\right)}{\left(1+\mathrm{Pr}_v\left(1-\frac{\theta}{\theta_r}\right)\right)^{4n}}E_C(f'')^2\frac{1}{\left(1-\frac{\theta}{\theta_r}\right)}$$

$$\left[1+Wef''\left(\frac{\mathrm{Pr}_v\left(1-\frac{\theta}{\theta_r}\right)}{\sqrt{2}\left(1+\mathrm{Pr}_v\left(1-\frac{\theta}{\theta_r}\right)\right)^{3n}}\right)\right]=0,$$

$$(20)$$
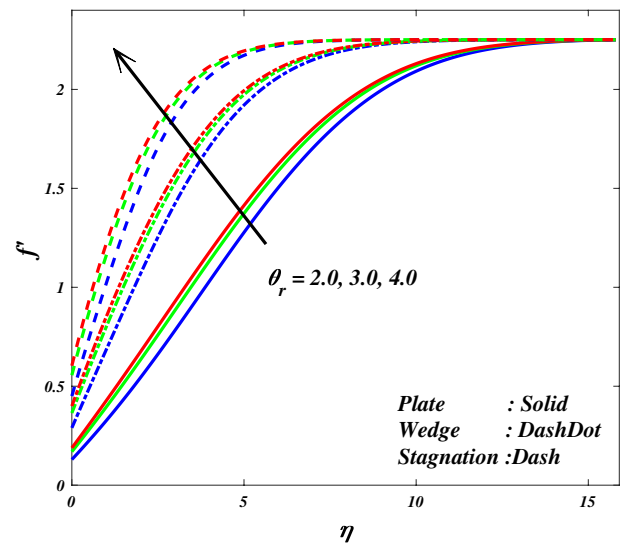
Fig. 2 f' for increasing values of θ_r

$$\chi''+\left(\frac{m+1}{2}\right)f\chi'\frac{Sc_v}{\mathrm{Pr}_v}+\frac{N_T}{N_B}\theta''=0. \qquad (21)$$

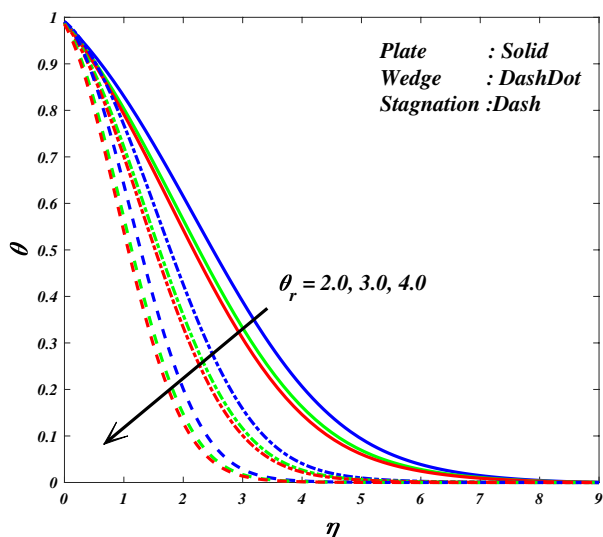The boundary conditions also transform as

Fig. 3 θ for increasing values of θ_r
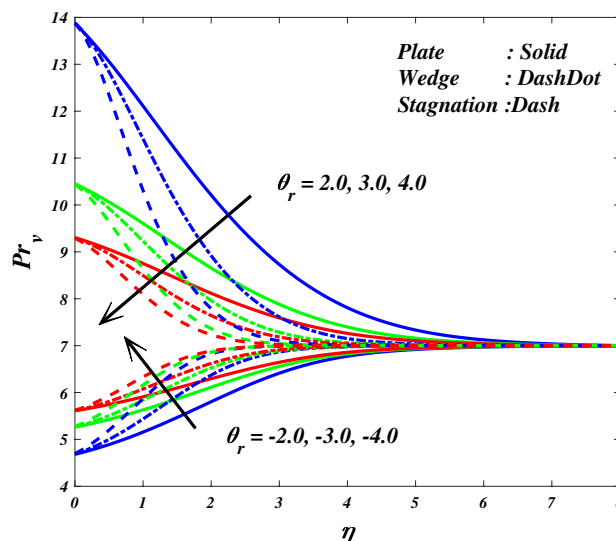
Fig. 4 Pr_v for increasing values of θ_r

$$f(\eta) = 0, f'(\eta) = \frac{\sqrt{Pr_v\left(1 - \frac{\theta}{\theta_r}\right)} K_s f''(\eta)}{\left(1 + Pr_v\left(1 - \frac{\theta}{\theta_r}\right)\right)^n}$$

$$\left(1 + \frac{We}{2} \frac{\sqrt{Pr_v\left(1 - \frac{\theta}{\theta_r}\right)} f''(\eta)}{\left(1 + Pr_v\left(1 - \frac{\theta}{\theta_r}\right)\right)^{3n}}\right),$$

$$\theta(\eta) = 1 + \frac{2\gamma}{\gamma+1} \frac{1}{\sqrt{Pr_v\left(1 - \frac{\theta}{\theta_r}\right)}} \frac{K_s \theta'(\eta)}{\left(1 + Pr_v\left(1 - \frac{\theta}{\theta_r}\right)\right)^n},$$

$$N_B \chi'(\eta) + N_T \theta'(\eta) = 0 \text{ at } \eta = 0,$$

$$f'(\eta) = \left(1 + Pr_v\left(1 - \frac{\theta}{\theta_r}\right)\right)^{2n}, \theta(\eta) \to 0, \chi(\eta) \to 0 \text{ as } \eta \to \infty.$$

$$(22)$$

The dimensionless local skin friction coefficient $\left(C_f^*\right)$, dimensionless local rate of heat transfer (Nu^*) and dimensionless local rate of mass transfer (Sh^*) at the wall are defined as

$$C_f^* Re^{1/2} = \frac{2 f''(0) \sqrt{Pr_v\left(1 - \frac{\theta}{\theta_r}\right)}}{\sqrt{1 + Pr_v\left(1 - \frac{\theta}{\theta_r}\right)}}$$

$$\left.\left(1 + \left(\frac{We}{2} f''(0) \frac{\sqrt{Pr_v\left(1 - \frac{\theta}{\theta_r}\right)}}{\left(1 + Pr_v\left(1 - \frac{\theta}{\theta_r}\right)\right)^{3n}}\right)\right)\right\}$$

$$Nu^* Re^{1/2} \delta^{-1} = -\theta'(0),$$

$$Sh^* Re^{1/2} \delta^{-1} = -\chi'(0).$$

$$(23)$$
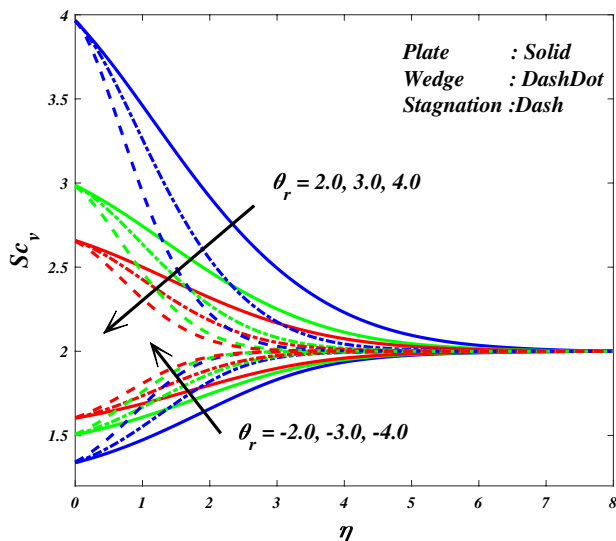
Fig. 5 Sc_v for increasing values of θ_r

3 Numerical method and code validation

Dimensionless Eqs. (19)–(21) with corresponding boundary conditions Eq. (22) have been solved by using RK Fehlberg scheme. The step size in the numerical solution is fixed as 0.001 ($\eta = 0.001$), and ten-decimal (1×10^{-10}) place accuracy is fixed for the criterion of convergence. To check the validity of the present model, the numerical results are compared with dsolve comment in Maple, which are given in Tables 1 and 2. It is noticed that the dsolve incorporated with midpoint is a Maple package which is widely employed to solve boundary value problems. The
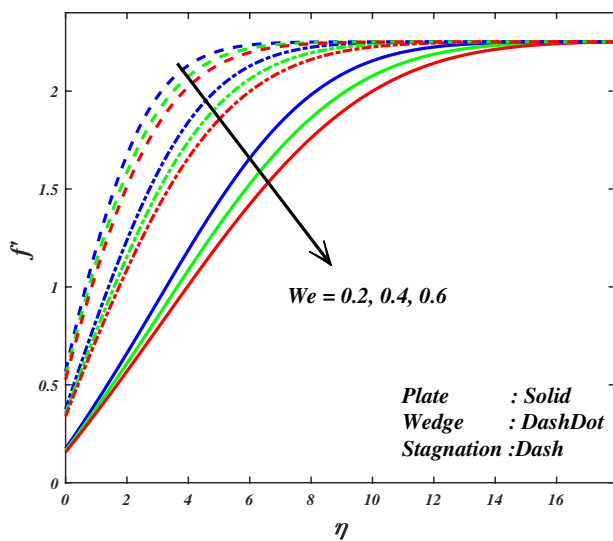
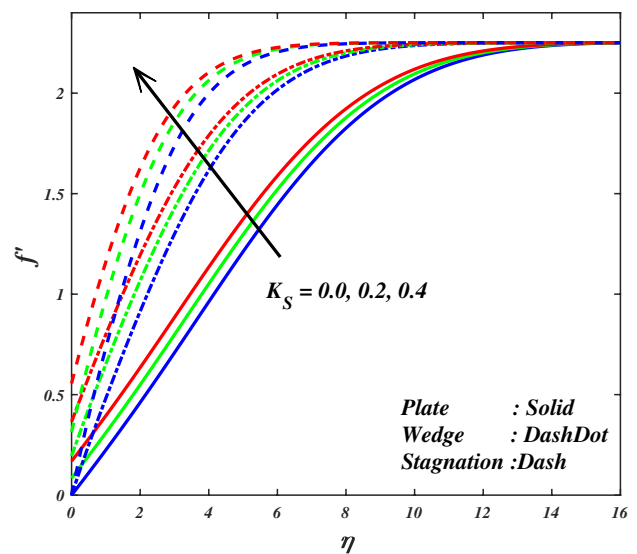**Fig. 6** f' for increasing values of We
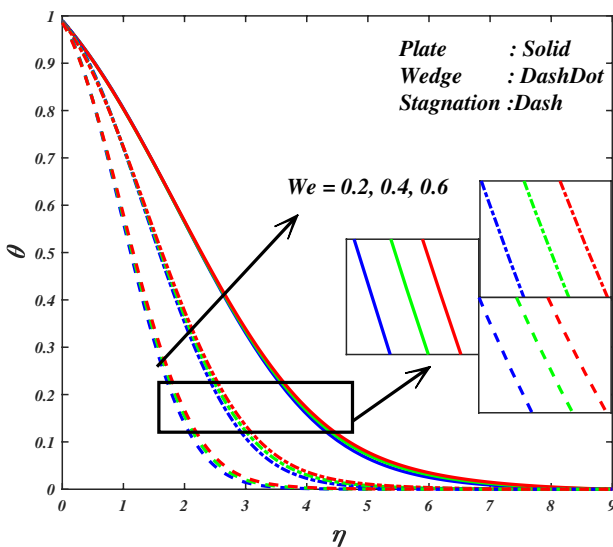

Fig. 8 f' for increasing values of K_S

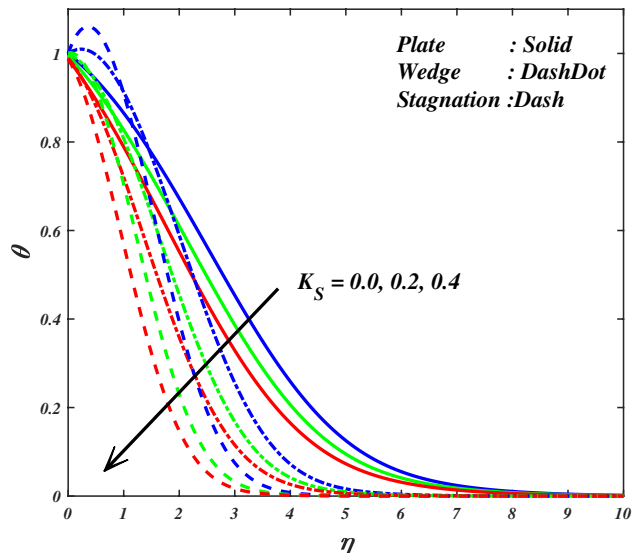**Fig. 7** θ for increasing values of We

Fig. 9 θ for increasing values of K_S

comparison results reported in Tables 1 and 2 received a good agreement. This evidences that the adopted numerical simulation gives precise results. The computation time of the dimensionless flow equations was evaluated using the "tic toc" command in MATLAB. It is observed that CPU has taken approximately 9–12 s to obtain the solution for flow over a plate, wedge and stagnation point cases using windows operating system with Intel Core i3 processor.

4 Results and discussion

The main goal of the present section is to exhibit the impact of active parameters like Weissenberg number ($We = 0.2, 0.4, 0.6$), variable viscosity parameter ($\theta_r = 2, 3, 4$), Brownian movement ($N_B = 0.3, 0.5, 0.8$), thermophoresis ($N_T = 0.1, 0.3, 0.5$) and slip parameter ($K_S = 0.0, 0.2, 0.4$) on velocity (f'), temperature (θ), concentration (χ), skin friction factor, rate of heat transfer and
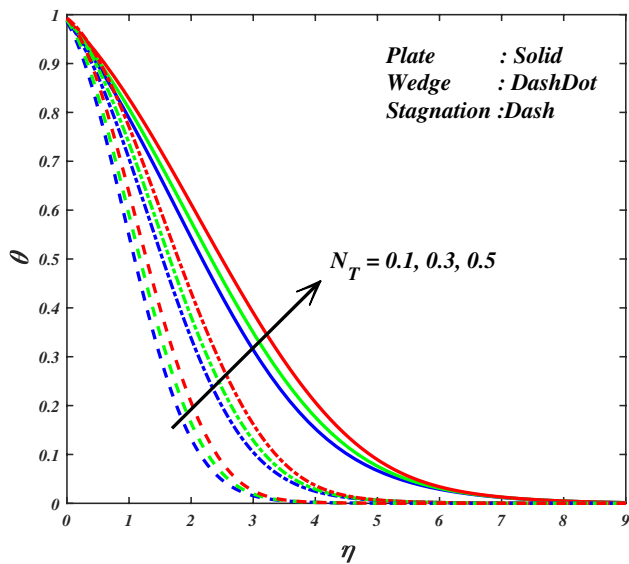
Fig. 10 θ for increasing values of N_T
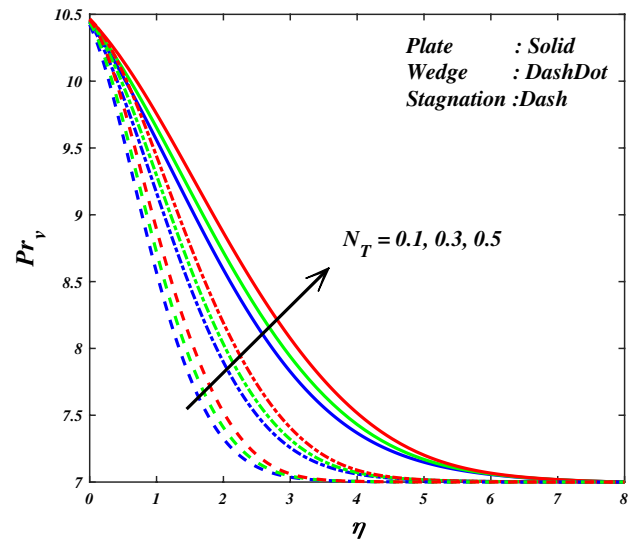

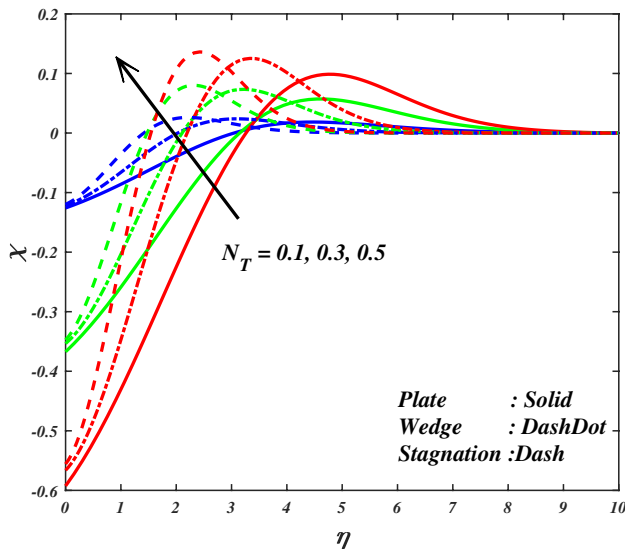**Fig. 12** Pr_v for increasing values of N_T

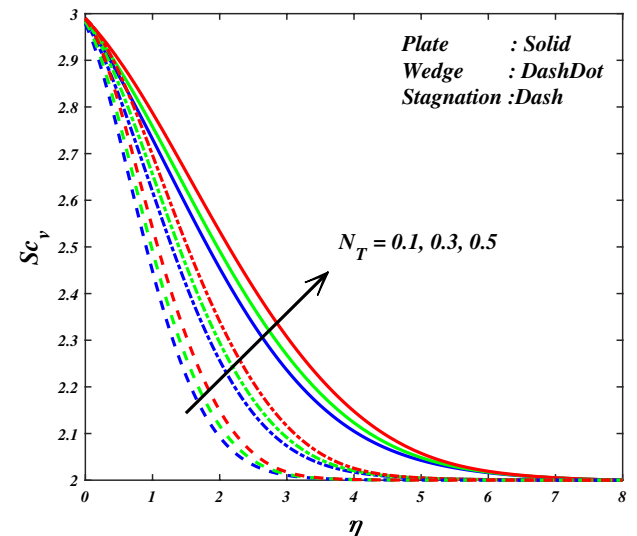**Fig. 11** χ for increasing values of N_T

Fig. 13 Sc_v for increasing values of N_T

rate of mass transfer via graphs. The value of the ambient Prandtl number (Pr_∞) and Schmidt number (Sc_∞) is taken as 7 and 2 when the Williamson nanofluid viscosity is not dependent on temperature. In this study, the viscosity of Williamson nanofluid is dependent on temperature, so that the variable Prandtl number and variable Schmidt number values are considered at the surface corresponding to 10.4112 and 2.9860, respectively, for $\theta_r = 3$. The non-dimensionalized governing flow equations subject to boundary conditions have been computed by RK Feldberg method. It is noteworthy that the results are obtained by taking $\beta_1 = 0$, 0.5 and 1.0 for the cases of plate, wedge

and stagnation point. Solid, dashdot, dash lines in order represent the Williamson nanofluid characteristics over a plate, wedge, and stagnation point. Figures 2, 3, 4, 5, 6, 7, 8, 9, 10, 11, 12, 13 and 14 depict the characteristics of fluid transport properties, and Figs. 18, 19, 20 and 21 illustrate the variable Prandtl number and rate of heat transfer for the cases wedge, plate and stagnation point.

Figures 2, 3 and 4 are plotted to explore the impact of θ_r on f', θ, Pr_v and Sc_v for the plate, wedge, and stagnation point cases, respectively. Figure 2 illustrates that f' increases with an increase in θ_r. It is vivid from this figure that for a larger value of θ_r, change in fluid velocity
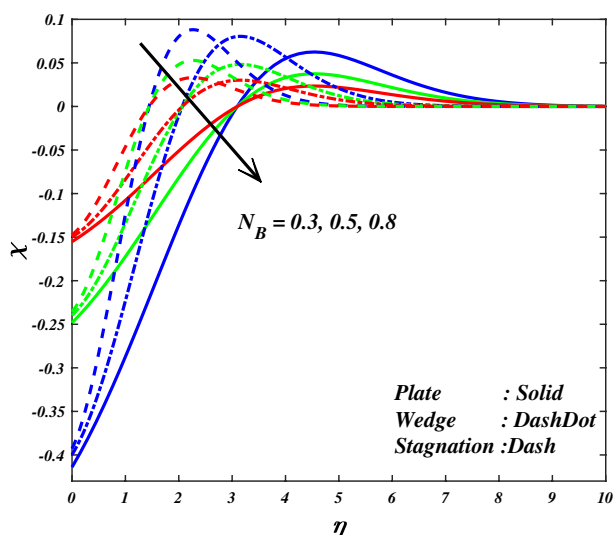
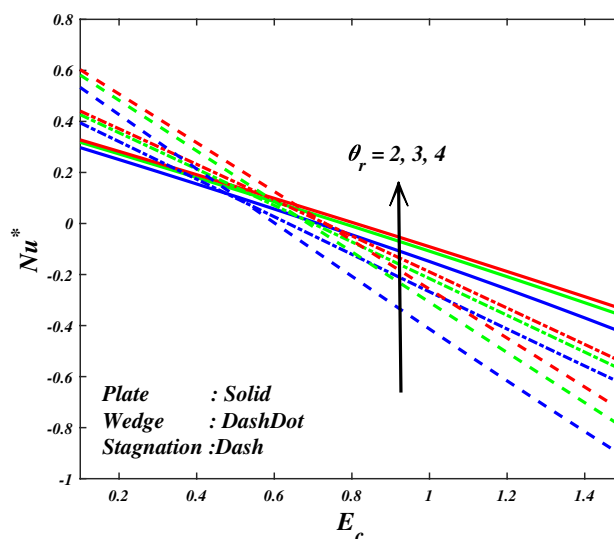**Fig. 14** χ for increasing values of N_B

Fig. 16 Nu^* for increasing values of E_C and θ_r
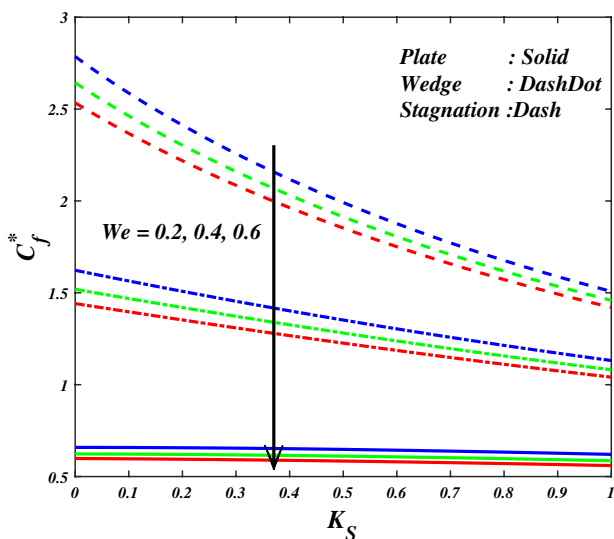

Fig. 15 C_f^* for increasing values of K_S and We
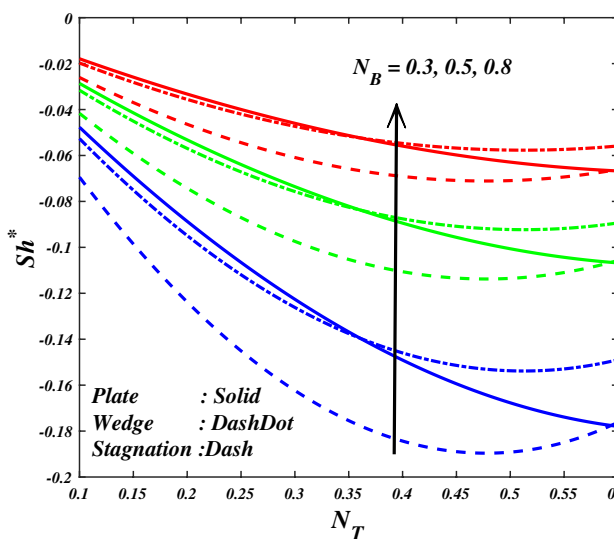

Fig. 17 Sh^* for increasing values of N_T and N_B

is negligible. Physically, when $\theta_r \to \infty$, fluid viscosity (μ_∞) and dynamic fluid viscosity (μ) are equal $(\mu_\infty = \mu)$ at the ambient temperature and this represents the case of the constant viscosity. Figure 3 depicts the effect of θ_r on θ. From these figures, it is found that θ lessens by uplifting values of θ_r and asymptote to zero as $\eta \to \infty$. This outcome also exhibits that when θ_r tends to a higher value, θ leads to decrease, because of $\mu \to \mu_\infty$ as $\theta_r \to \infty$. The graph in Fig. 4 shows that a rise in θ_r results in decline in Pr_v, whereas it is the opposite behavior for negative values of θ_r. It is seen from figure that variable Prandtl number asymptotically converges with the value of an ambient

Prandtl number at $\eta \to \infty$. The reason for that is an increment in θ_r provokes the surface of the plate, wedge and stagnation Pr_v to approach Pr_∞. Through Fig. 5, the augmentation of Sc_v is reported for positive and negative values of θ_r. It is evident that Sc_v manifests a similar character of Pr_v. Furthermore, it is noticed that there are decays in Sc_v by increasing θ_r, whereas there is an enhancement of Sc_v for negative values of θ_r.

f' and θ for distinct values of We are depicted in Figs 6 and 7 for the plate, wedge, and stagnation point cases, respectively. From these figures, it is seen that the fluid velocity diminishes for growing values of We, whereas it
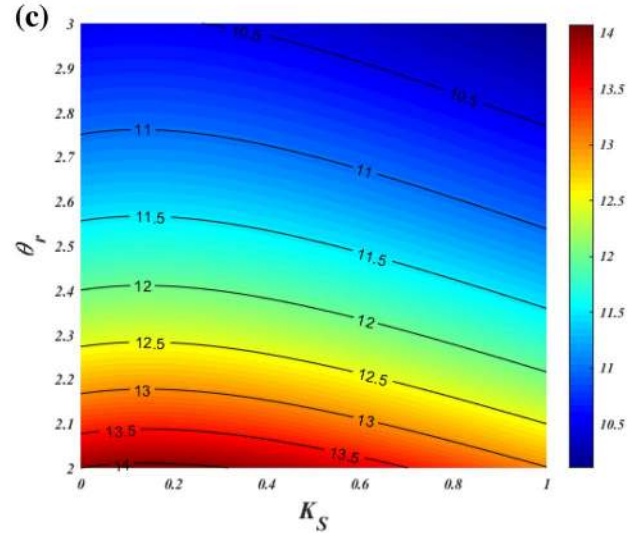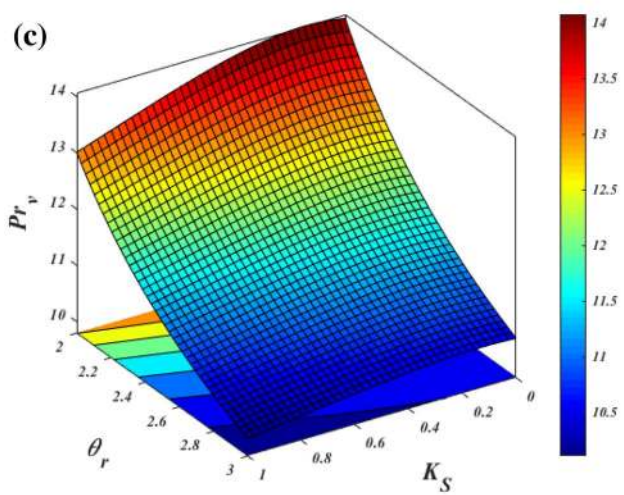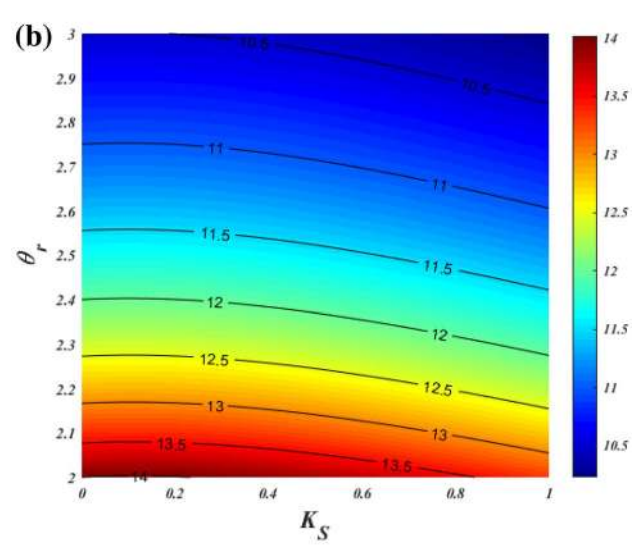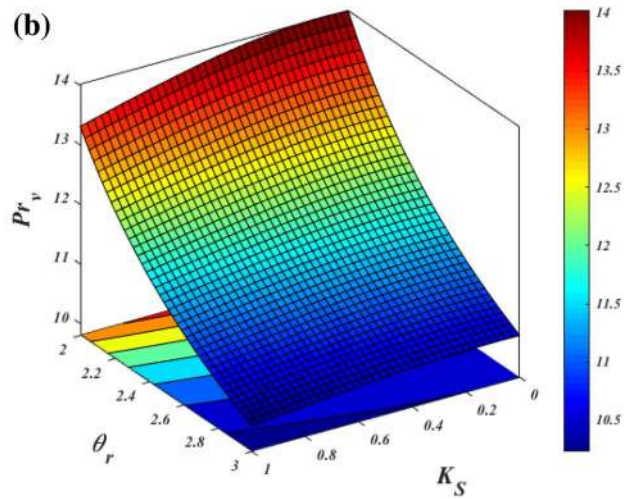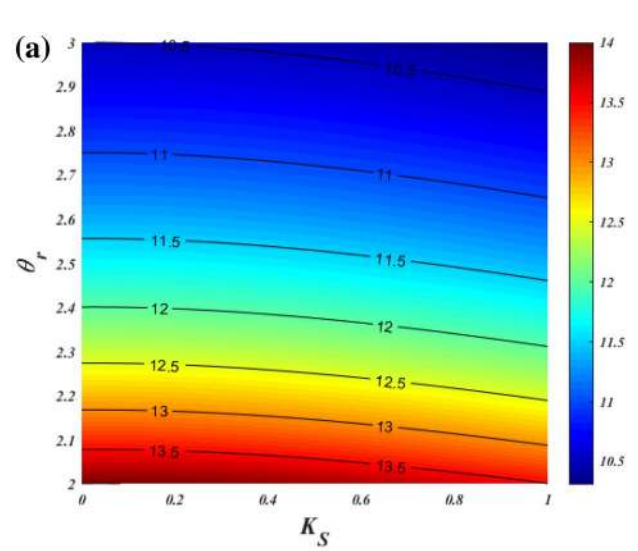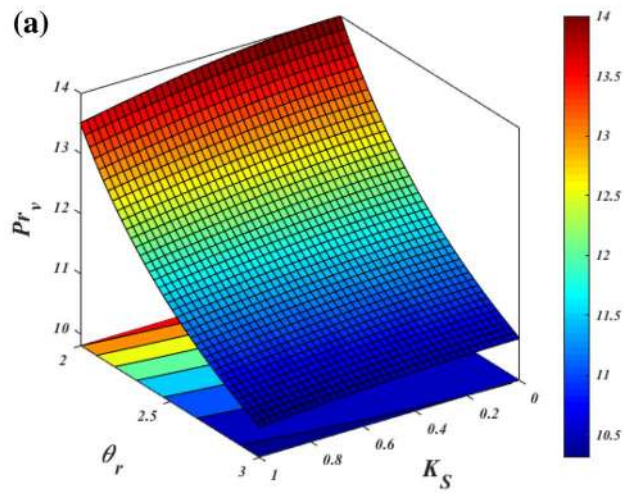
Fig. 18 3D plot and contour with the impact of θ_r and K_S on Pr_v for Williamson nanofluid when $\beta_1 = 0, 0.5, 1$

Fig. 19 Contour with the impact of θ_r and K_S on Pr_v for Williamson nanofluid when $\beta_1 = 0, 0.5, 1$
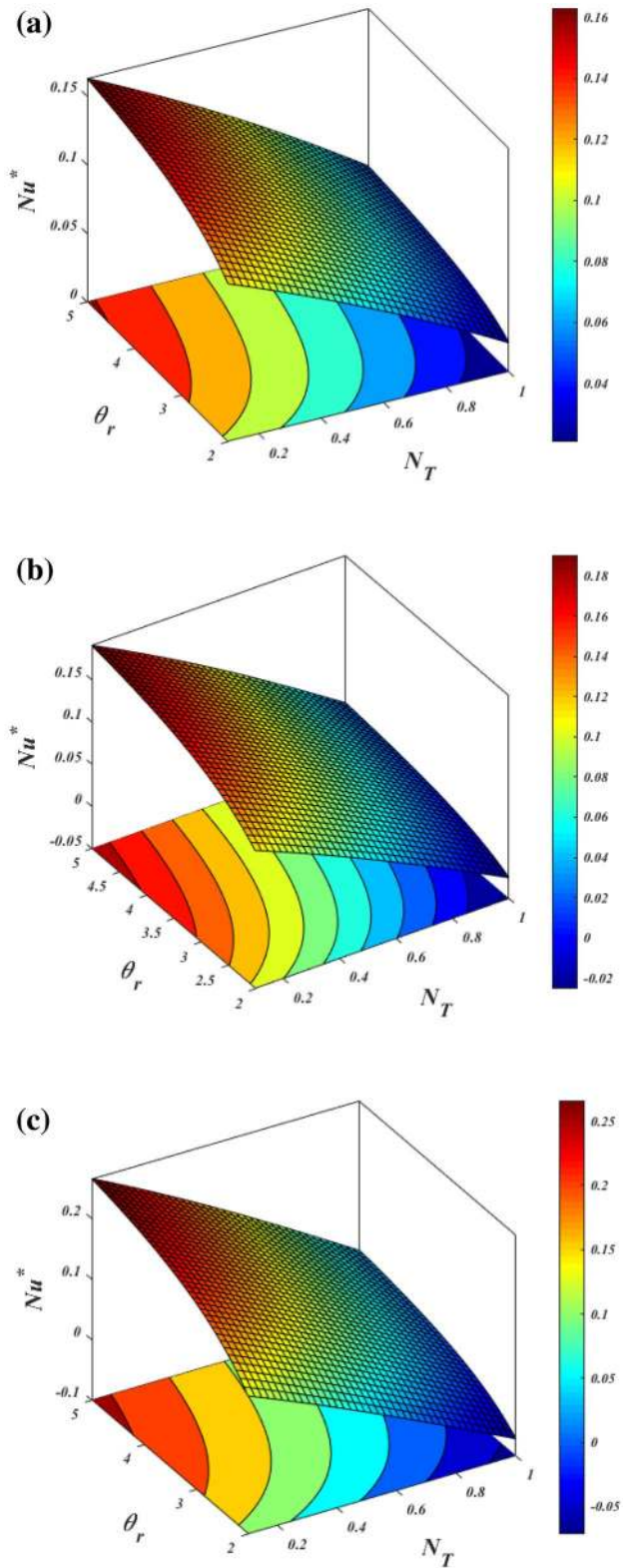
Fig. 20 3D plot and contour with the impact of θ_r and N_T on Nu^* for Williamson nanofluid when $\beta_1 = 0, 0.5, 1$
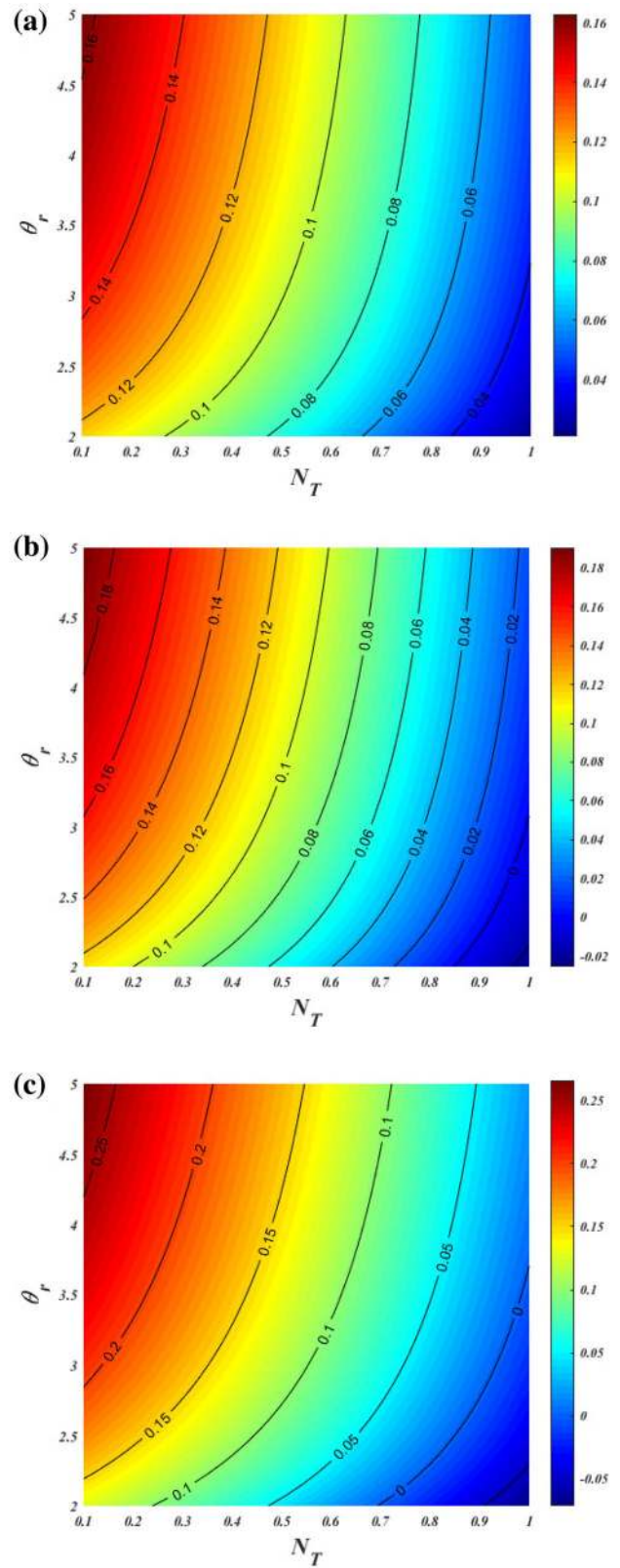
Fig. 21 Contour with the impact of θ_r and N_T on Nu^* for Williamson nanofluid when $\beta_1 = 0, 0.5, 1$

is the reverse nature in temperature. An increment in the value of We tends to enlarge material relaxation time, and thus the velocity of the Williamson nanofluid lessens and the Williamson nanofluid temperature enhances. Figures 8 and 9 exhibit the influence of K_S on f' and θ for the cases of plate, wedge and stagnation. An increasing trend in f' is depicted for higher values of K_S. It is noticed that while $K_S = 0$, the surface of the boundary represents no slip. As the nanofluid flow becomes more rarefied, the surface friction reduces, resulting in an increase in the nanofluid velocity. Hence, the nanofluid velocity enhances with the increases in rarefaction influence whether the nanofluid characteristics are variable or constant. Figure 9 portrays how K_S affects θ. There is a decay in θ when K_S is rising because of the strong rarefaction highly diminishing the surface θ. Figures 10 and 11 demonstrate the effect of N_T on θ, χ, Pr_v and Sc_v for plate, wedge, and stagnation point cases, respectively. The thermophoretic force generated as a result of the temperature gradient leads to rapid flow beyond from the plate, wedge and stagnation. Hence, the heated fluid is moved beyond the surfaces of the plate, wedge and stagnation. As a result, the thermal-related boundary layer rises with N_T increase. Variation of N_T on χ is illustrated in Fig. 11. It is evident from this figure that χ increases with higher values of N_T. The thermophoresis force triggers the nanoparticles to move from the hot surface to the cold surface which causes the mass-related boundary layer thickness to upsurge. The variation of the Pr_v and Sc_v is represented through Figs. 12 and 13 for distinct values of N_T. It is found that both the figures show an increasing behavior for uplifted values of N_T. Figure 14 displays the results for Williamson nanofluid χ for distinct values of N_B. It is seen from the figure that χ shows decreasing behavior over the plate, wedge and stagnation as N_B increases. Brownian movement occurs in nanofluid systems due to contact of nanoparticles with the base fluid. This leads to enhancing the heat conduction, and hence the concentration boundary layer thickness diminishes.

Figure 15 shows the impacts of We and K_S on C_f^*. It is observed that C_f^* of Williamson nanofluid at the surface reduces by augmenting K_S. It is shown that increasing values of We declines C_f^* of Williamson nanofluid over a plate, wedge and stagnation point cases. Figure 16 is drawn to explore the influence of θ_r on Nu^* against E_C. It is noticed that Nu^* of nanofluid at the surfaces of the plate, wedge and stagnation point enhances by enhancing θ_r. However, an increase in E_C restricts the augments of Nu^* at the surface. Figure 17 displays the influences of N_T and N_B parameters on the rate of mass transfer. It is evident that the rate of mass transfer declines at the surface by enhancing N_T. It is also noticed that N_B increases the rate of mass transfer. Figures 18 and 19 elucidated Pr_v for various values of θ_r and K_S over the plate, wedge and stagnation point. It is

noticed that the Pr_v is a decreasing function of θ_r and K_S. Figures 20 and 21 are drawn to explore the influence of θ_r on Nu^* against N_T, respectively. It is manifested that θ_r and N_T have an opposite trend on Nu^* over a plate, wedge and stagnation point.

5 Conclusion

The present communication has been carried out to examine the variable viscosity, variable Prandtl number and variable Schmidt number impacts on Williamson nanofluid over a plate, wedge and stagnation point. A Williamson model has been employed to explore the flow characteristics in the presence of heat and mass transfer. The RK method has implemented to elucidate the governing flow-field mathematical equations. The outcomes are demonstrated in terms of 2-dimensional plot, 3-dimensional surface plot and contour plot. Key points of the present analysis are listed below.

- Larger values of variable viscosity parameter enhance the nanofluid velocity and lessen the temperature.
- Variable Prandtl number and variable Schmidt number exhibit a similar behavior for variable viscosity parameter.
- Weissenberg number has the opposite behavior on nanofluid velocity and temperature.
- An increment of the slip parameter and thermophoresis enhance the temperature.
- The plate contains higher fluid temperature than the wedge and stagnation point cases.
- Thermophoresis parameter and Brownian motion parameter on the concentration profile are reverse in nature.
- Compared to wedge and stagnation point, the plate has less skin friction factor and rate of heat transfer.

Compliance with ethical standards

References

1. Choi SUS, Eastman JA (1995) Enhancing thermal conductivity of fluids with nanoparticles. In: Proceedings of the 1995 ASME international mechanical engineering congress and exposition, 1217 November (American Society of Mechanical Engineers,

fluids engineering division (publication) FED, 1995) vol 231. San Francisco, California pp 99–105

2. Buongiorno J (2006) Convective transport in nanofluids. J Heat Transfer 128:240

3. Animasaun IL, Ibraheem RO, Mahanthesh B, Babatunde HA (2019) A meta-analysis on the effects of haphazard motion of tiny/nanosized particles on the dynamics and other physical properties of some fluids. Chin J Phys 60:676–687

4. Wakif A, Animasaun IL, Satya Narayana PV, Sarojamma G (2019) Meta analysis on thermo-migration of tiny/nano-sized particles in the motion of various fluids. Chin J Phys. https://doi.org/10.1016/j.cjph.2019.12.002

5. Khan MI, Qayyum S, Hayat T, Khan MI, Alsaedi A, Ahmad T (2018) Entropy generation in radiative motion of tangent hyperbolic nanofluid in presence of activation energy and nonlinear mixed convection. Phys Lett A 382:2017–2026

6. Ghadikolaei SS, Hosseinzadeh K, Ganji DD (2019) Investigation on magneto Eyring–Powell nano fluid flow over inclined stretching cylinder with nolinear thermal radiation and Joule heating effect. World J Eng 16:51–63

7. Ahmed J, Khan M, Ahmad L (2019) Stagnation point flow of Maxwell nanofluid over a permeable rotating disk with heat source/sink. J Mol Liq 287:110853

8. Das K, Acharya N, Kundu PK (2018) Influence of variable fluid properties on nanofluid flow over a wedge with surface slip. Arab J Sci Eng 43:2119–2131

9. Makinde OD, Aziz A (2011) Boundary layer flow of a nanofluid past a stretching sheet with a convective boundary condition. Int J Therm Sci 50:1326–1332

10. Basha HT, Sivaraj R, Animasaun IL, Makinde OD (2018) Influence of non-uniform heat source/sink on unsteady chemically reacting nanofluid flow over a cone and plate. Defect Diffus Forum 389:50–59

11. Dabe NT, Attia HA, Essawy MAI, Abdelmaksoud IH, Ramadan AA, Hamid AHA (2019) Non-linear heat and mass transfer in a thermal radiated MHD flow of a power-law nanofluid over a rotating disk. SN Appl Sci 1:551

12. Kandasamy R, Adnan NA, Radiah M, Kamarulzaki M (2019) Electric field strength on MHD aluminum alloys (AA7075) nanofluid flow. SN Appl Sci 1:12

13. Kumar BR, Sivaraj R (2013) Heat and mass transfer in MHD viscoelastic fluid flow over a vertical cone and flat plate with variable viscosity. Int J Heat Mass Transf 56:370–379

14. Sivaraj R, Kumar BR (2012) Unsteady MHD dusty viscoelastic fluid Couette flow in an irregular channel with varying mass diffusion. Int J Heat Mass Transf 55:3076–3089

15. Manjunatha G, Rajashekhar C, Vaidya H, Prasad KV, Vajravelu K (2020) Impact of heat and mass transfer on the peristaltic mechanism of Jeffery fluid in a non-uniform porous channel with variable viscosity and thermal conductivity. J Therm Anal Calorim 139:1213–1228

16. Mythili D, Sivaraj R (2016) Influence of higher order chemical reaction and non-uniform heat source/sink on Casson fluid flow over a vertical cone and flat plate. J Mol Liq 216:466–475

17. Benazir AJ, Sivaraj R, Rashidi MM (2016) Comparison between Casson fluid flow in the presence of heat and mass transfer from a vertical cone and flat plate. J Heat Transf 138:112005

18. Williamson RV (1929) The flow of pseudoplastic materials. Ind Engr Chem Res 11:1108–1111

19. Abegunrin OA, Okhuevbie SO, Animasaun IL (2016) Comparison between the flow of two non-Newtonian fluids over an upper horizontal surface of paraboloid of revolution: boundary layer analysis. Alex Eng J 55:1915–1929

20. Hashim A, Hamid M, Khan M (2018) Unsteady mixed convective flow of Williamson nanofluid with heat transfer in the presence of variable thermal conductivity and magnetic field. J Mol Liq 260:436–446

21. Abegunrin OA, Animasaun IL (2017) Motion of Williamson fluid over an upper horizontal surface of a paraboloid of revolution due to partial slip and buoyancy: boundary layer analysis. Defect Diffus Forum 378:16–27

22. Khan M, Salahuddin T, Malik MY, Mallawi FO (2018) Change in viscosity of Williamson nanofluid flow due to thermal and solutal stratification. Int J Heat Mass Transf 126:941–948

23. Jones AD, Buie CR (2019) Continuous shear stress alters metabolism, mass-transport, and growth in electroactive biofilms independent of surface substrate transport. Sci Rep 9:1–8

24. Prasad RC, Shen J (1994) Performance evaluation using exergy analysis-application to wire-coil inserts in forced convection heat transfer. Int J Heat Mass Transf 37:2297–2303

25. Fodemski TR (1992) Forced convection film boiling in the stagnation region of a molten drop and its application to vapour explosions. Int J Heat Mass Transf 35:2005–2016

26. Basha HT, Sivaraj R, Reddy AS, Chamkha AJ (2019) SWCNH/diamond-ethylene glycol nanofluid flow over a wedge, plate and stagnation point with induced magnetic field and nonlinear radiation -solar energy application. Eur Phys J Special Top 228:2531–2551

27. Lin HT, Lin LK (1987) Similarity solutions for laminar forced convection heat transfer from wedges to fluids of any Prandtl number. Int J Heat Mass Transf 30:1111–1118

28. Bianco V, Chiacchio F, Manca O, Nardini S (2009) Numerical investigation of nanofluids forced convection in circular tubes. Appl Therm Eng 29:3632–3642

29. Sheikholeslami M (2017) Magnetohydrodynamic nanofluid forced convection in a porous lid driven cubic cavity using lattice Boltzmann method. J Mol Liq 231:555–565

30. Rahman ATMM, Alam MS, Chowdhury MK (2012) Thermophoresis particle deposition on unsteady two-dimensional forced convective heat and mass transfer flow along a wedge with variable viscosity and variable Prandtl number. Int Commun Heat Mass Transf 39:541–550

31. Chamkha AJ, Mujtaba M, Quadri A, Issa C (2003) Thermal radiation effects on MHD forced convection flow adjacent to a non-isothermal wedge in the presence of a heat source or sink. Heat Mass Transf 39:305–312

32. Uddin MJ, Khan WA, Ismail AI (2015) Effect of variable properties, Navier slip and convective heating on hydromagnetic transport phenomena. Indian J Phys 90:627–637

33. Rashidi MM, Nasiri M, Shadloo MS, Yang Z (2017) Entropy generation in a circular tube heat exchanger using nanofluids: effects of different modeling approaches. Heat Transf Eng 38:853–866

34. Ma Y, Mohebbi R, Rashidi MM, Yang Z (2018) Study of nanofluid forced convection heat transfer in a bent channel by means of lattice Boltzmann method. Phys Fluids 30:032001

35. Mohebbi R, Rashidi MM, Izadi M, Sidik NAC, Xian HW (2018) Forced convection of nanofluids in an extended surfaces channel using lattice Boltzmann method. Int J Heat Mass Transf 117:1291–1303